RSC Advances

PAPER

View Article Online
View Journal | View Issue

Cite this: *RSC Adv.*, 2021, **11**, 9021

Rapid and sensitive determination of doxorubicin in human whole blood by vertically-ordered mesoporous silica film modified electrochemically pretreated glassy carbon electrodes†

Meifang Wang,‡[a] Jing Lin,‡[b] Jiawei Gong,[a] Mingchen Ma,[c] Hongliang Tang,*[d] Jiyang Liu[a] and Fei Yan*[a]

Direct and accurate detection of doxorubicin (DOX) in unprocessed human whole blood is of vital importance in medical diagnosis and monitoring. In this work, we demonstrate the utilization of electrochemically pretreated glassy carbon electrodes (p-GCE) modified with vertically-ordered mesoporous silica films (VMSF) for rapid and sensitive electrochemical detection of DOX. The electrochemically pretreated process is a simple, cost-effective and environmentally friendly approach for improving interface catalytic properties and introducing oxygen-containing groups into the GCE surface, which could be suitable for stably growing VMSF without any adhesive layer simultaneously retaining the underlying electrode activity. Benefiting from the highly sensitive electrode substrate of p-GCE and electrostatic preconcentration effect of VMSF, the present VMSF/p-GCE sensor was able to determine DOX with an ultrahigh sensitivity (23.94 μA μM^{-1}) and a relatively low limit of detection (0.2 nM) and a rather wide linear range (0.5 nM to 23 μM). Furthermore, direct and reliable electrochemical detection of DOX in human whole blood without complicated sample pretreatments was achieved owing to the excellent anti-fouling and anti-interference ability of VMSF.

Received 25th November 2020
Accepted 8th February 2021

DOI: 10.1039/d0ra10000e

rsc.li/rsc-advances

1. Introduction

DOX is an anthracycline molecule widely used as anti-cancer and antitumoral drugs in clinical diagnosis and therapy.[1] Although DOX is an efficient kind of chemotherapeutic drugs, long-term use of DOX will produce adverse side effects, such as intercalation into DNA with inhibition of macromolecular biosynthesis[2,3] and formation of free radicals with induction of DNA damage or alkylation.[4,5] And the actual DOX concentration in human blood samples is closely related to the clinical effectiveness of treatment and patient safety. Therefore, rapid and accurate determination of the DOX level in human blood samples is of great significance. Several analytical approaches have been developed to detect DOX, such as high-performance liquid chromatography (HPLC),[6,7] fluorimetry,[8] liquid chromatography coupled with mass spectrometry[9,10] or electrochemical techniques.[11,12] Among them, electrochemical methods have been recently recognized as potential and practical tools due to their simple operation, low cost, sensitive response and real-time detection. However, surface fouling in biofluids, especially in human whole blood, is unavoidable due to the undesirable adsorption of biological species (*e.g.* polysaccharides, lipids, proteins, cells and some microorganisms), hindering the effective electron transfer and signal transduction process and thus affecting the sensitivity, reproducibility and reliability of the sensors.[13–16]

Vertically-ordered mesoporous silica films (VMSF) emerged as a kind of anti-fouling and anti-interference electrode modifier have received ever-increasing attention due to their well-ordered nanochannels, uniform pore size, ultrathin thickness, and high pore density.[17–20] Such VMSF material with opening nanochannels perpendicularly aligned to the electrode surface can prevent the physical contact between the fouling agents and the underlying electrode, providing a simple and rapid platform for direct electrochemical analysis of complex samples.[21–26] They are often prepared on the solid electrode substrates (*e.g.* indium tin oxide (ITO), gold, platinum, and glassy carbon electrode (GCE)) by using Stöber-solution growth[27] and

[a]*Department of Chemistry, Zhejiang Sci-Tech University, 928 Second Avenue, Xiasha Higher Education Zone, Hangzhou 310018, PR China. E-mail: feifei19881203@126.com*

[b]*The First Affiliated Hospital of Guangxi University of Chinese Medicine, Nanning 530023, China*

[c]*Guangxi University of Chinese Medicine, Nanning 530020, China*

[d]*Affiliated Fangchenggang Hospital, Guangxi University of Chinese Medicine, Fangchenggang 538001, China. E-mail: tanghl2004@gxtcmu.edu.cn*

† Electronic supplementary information (ESI) available: More details of optimized conditions for DOX detection and DPVs of DOX in human whole blood. See DOI: 10.1039/d0ra10000e

‡ The two authors contributed equally.

electrochemically assisted self-assembly (EASA) approaches.[28,29] In comparison with the ITO electrode, GCE is a widespread and electrochemically active carbonaceous electrode but often encounters the poor adhesion issues when VMSF attaches to the electrode surface, limiting the practical application. Organosilanes including mercaptopropyltrimethoxysilane and 3-aminopropyltriethoxysilane (APTES) have been reported to serve as the molecular glues to improve the adhesion of VMSF on the gold or GCE, but meanwhile electrode passivation will be come into play.[30–32] As we shall show in recent works, reduced graphene oxide (rGO) sheets modified GCE not only enable stable growth of VMSF based on the formed covalent bonding between oxygen-containing groups of rGO and silanol groups, but also act as an electroactive layer to further promote the electroanalytical performance.[33,34] However, exploitation of such adhesive layers requires more chemical materials, complex steps and elaborate operations for uniform modification.

Electrochemical pretreatment is a simple, low-cost, and environmentally-friendly approach to activate electrode surface and displays more pronounced effect to the carbonaceous electrodes, resulting in the fast reaction kinetics and highly reproducible physiochemical characteristics.[35] As compared with other activated techniques including mechanical polishing,[36] solvent cleaning,[36] vacuum heat treatment,[37] laser-based thermal treatment,[38] microwave plasma treatment,[39] and radio-frequency plasma treatment,[40] electrochemical pretreatment is fascinating and the pretreated carbonaceous electrodes have been directly and extensively used for sensitive electroanalysis of various analytes from environmental pollutants, drugs to neurotransmitters.[41–43] It has been found that new active defects/edge plane sites and oxygen-containing groups produced in the process of electrochemical pretreatment play important roles in accelerating the rate of electron transfer, remarkably increasing the highly electrochemical activity and excellent electrocatalytic activity of the electrodes.[44,45] Moreover, electrochemical pretreatment process provides the electrode with rough surface and more functional groups, which could be utilized to modify with other specific materials to further improve selectivity and sensitivity of the electrodes.[46]

In this work, we demonstrated a direct and sensitive electrochemical approach for the detection of DOX in human whole blood by modifying the electrochemically pretreated glassy carbon electrode (p-GCE) with VMSF. Such obtained VMSF/p-GCE sensor could not only detect DOX with high sensitivity due to the superior electrocatalytic activity of p-GCE and electrostatic enrichment effect of nanochannels, but also realize the rapid and anti-fouling determination of DOX in complex human blood sample owing to the excellent anti-fouling and anti-interference of VMSF. In comparison with bare GCE, VMSF/p-GCE presents more sensitive electrochemical performance, which is very suitable for trace analysis. Furthermore, owing to the oxygen-containing groups of p-GCE, the VMSF can be simply and stably prepared on the p-GCE by the electrochemically assisted self-assembly method in several seconds without any adhesive layer, making the sensor more promising for practical applications.

2. Materials and methods

2.1 Chemicals and materials

DOX, tetraethoxysilane (TEOS), cetyltrimethylammonium bromide (CTAB), potassium ferricyanide ($K_3[Fe(CN)_6]$), potassium ferrocyanide ($K_4[Fe(CN)_6]$), glucose (Glu), citric acid (CA), L-leucine (Leu), L-threonine (Thr), glycine (Gly), acetaminophen (APAP), ascorbic acid (AA), uric acid (UA), and dopamine (DA) were purchased from Aladdin. Sodium nitrate ($NaNO_3$) was bought from Wuxi Zhangwang Chemical Reagent. Ethanol (99.8%) and sodium hydroxide (NaOH) were obtained from Hangzhou Gaojing chemical reagent. Hydrochloric acid (HCl) was bought from Hangzhou Shuanglin Chemical Reagent. Phosphate buffer solutions (PBS) were prepared by mixing NaH_2PO_4 and Na_2HPO_4 in certain ratio. Human whole blood samples were obtained from the Center for Disease Control and Prevention (Hangzhou, China) approved by the Ethical Review Board of Zhejiang Sci-Tech University. All chemicals and reagents were directly used as received without further purification. Ultrapure water (18.2 MΩ cm) was used to prepare all aqueous solutions throughout this experiment.

2.2 Preparation of VMSF/p-GCE

GCE of 3.0 mm diameter was polished with 0.3 μm and 0.05 μm alumina slurries sequentially on polishing cloth and then ultrasonicated cleanly in ultrapure water for 1 min prior to use. Subsequently, the freshly cleaned GCE was electrochemically pretreated by applying +1.8 V for 300 s in 0.1 M PBS (pH = 5.0), followed by −1.0 V for 60 s according to the previous report.[45] After being rinsed with water and dried under a N_2 stream, electrochemically pretreated GCE was obtained, designated as the p-GCE.

The VMSF was grown on the p-GCE by using the EASA method as previously reported.[29] Typically, a precursor solution composed of 20 mL ethanol, 20 mL $NaNO_3$ (0.1 M, pH = 2.6), 1.585 g CTAB and 2.833 g TEOS was pre-hydrolyzed under stirring at room temperature for 2.5 h. Subsequently, a current density (-0.74 mA cm^{-2}) was applied to the p-GCE for 10 s with an Ag/AgCl (saturated KCl) as the reference electrode and a stainless steel plate as the counter electrode. The resulting electrode was immediately rinsed with large amounts of water, dried under a N_2 stream and finally aged overnight at 80 °C. Thus, VMSF with surfactant micelles (SM) confined in the silica nanochannels was formed on the p-GCE, termed as SM@VMSF/p-GCE. Extraction of SM was achieved by treating SM@VMSF/p-GCE with 0.1 M HCl–ethanol solution under stirring for 5 min, to obtain VMSF/p-GCE.

2.3 Measurements and instrumentations

Transmission electron microscopy (TEM) measurements were carried out using a HT7700 transmission electron microscope (Hitachi, Japan) at an acceleration voltage of 100 kV. The TEM specimen was prepared by carefully peeling off the VMSF from p-GCE surface, dispersing them in ethanol under ultrasonication before dropping onto copper grids. Scanning electron microscopy (SEM) images were obtained on

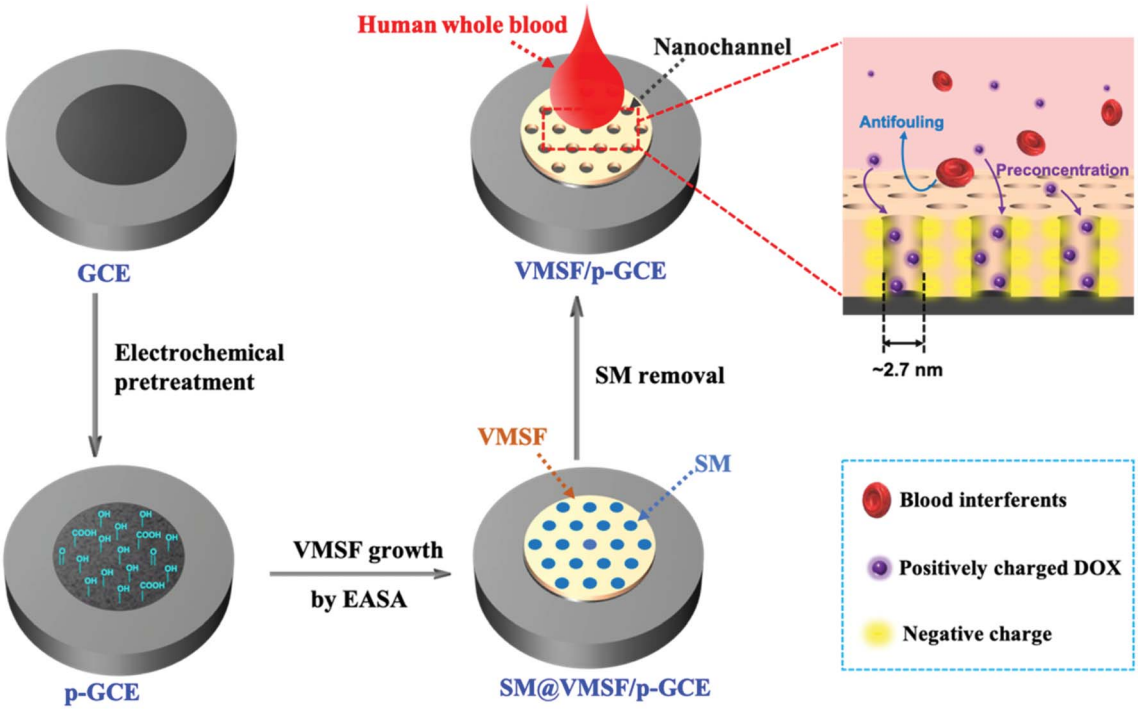

Scheme 1 Illustration of the preparation of the VMSF/p-GCE.

a GeminiSEM500 Scanning electron microscope (ZEISS, Germany) operated at 3.0 kV. X-Ray photoelectron spectroscopy (XPS) analysis was taken on a PHI5300 electron spectrometer using 250 W, 14 kV, Mg Kα radiation (PE Ltd, USA). Contact angle images were recorded by using a DSA 10-MK2 contact angle system (Kruss, Germany). Electrochemical impedance spectroscopy (EIS), cyclic voltammetry (CV) and differential pulse voltammetry (DPV) measurements were performed on an Autolab PGSTAT302N electrochemical workstation (Metrohm, Switzerland) at room temperature, using a conventional three electrodes system with an Ag/AgCl electrode as the reference electrode, a platinum electrode as the counter electrode and a bare or modified GCE as the working electrode. The DPV parameters used were as follows: step, 0.005 V; modulation amplitude, 0.05 V; modulation time, 0.05 s; interval time, 0.2 s.

3. Results and discussion

3.1 Characterizations of VMSF/p-GCE

Scheme 1 illustrates the preparation of the VMSF/p-GCE by combining the electrochemical pretreatment and electrochemically assisted self-assembly (EASA) methods. As shown, GCE was firstly treated with electrochemical pretreatment, which could not only achieve sensitive electrode surface but also incorporate the oxygen-containing functional groups onto the GCE surface, to obtain electrochemically pretreated GCE (p-GCE). As characterized by contact angle, oxygen-containing groups were generated on the electrode surface after electrochemical pretreatment (Fig. S1†). Incorporation of oxygen-functional groups on the GCE surface was further proofed by XPS. The results show that the intensities of C–O and O–C=O obviously increased, suggesting the abundant –OH groups

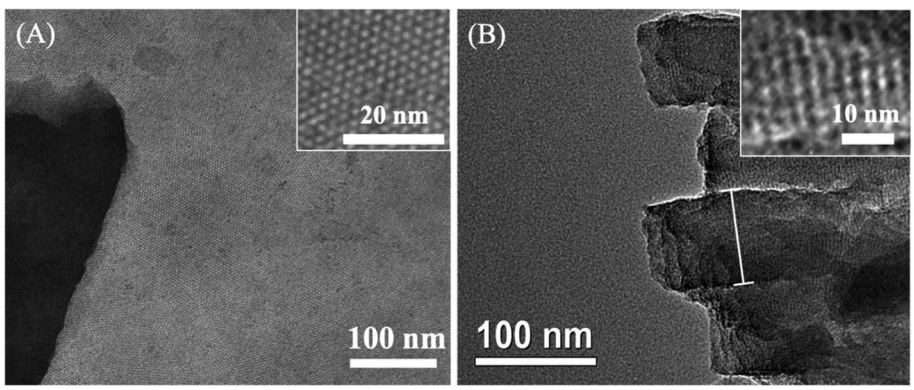

Fig. 1 (A) Top-view and (B) cross-section view TEM images of VMSF. The inset in (A) is the magnified images of top-view TEM.

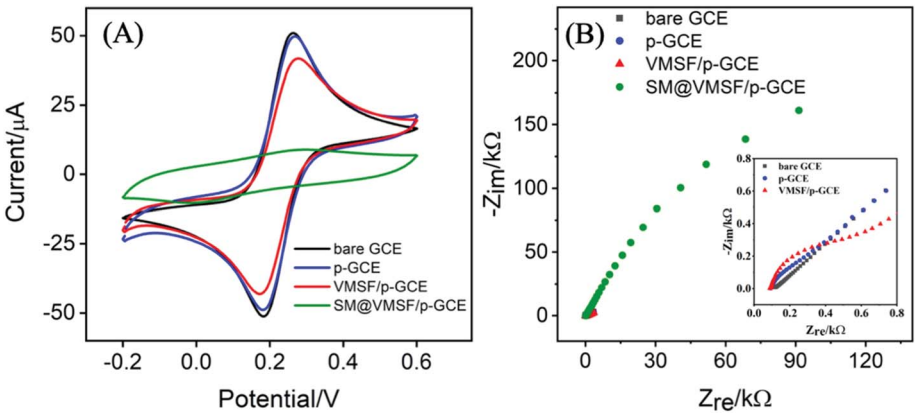

Fig. 2 CV (A) and EIS (B) plots of the bare GCE, p-GCE, VMSF/p-GCE and SM@VMSF/p-GCE in 0.1 M KCl solution containing 2.5 mM $Fe(CN)_6^{3-/4-}$. The scan rate in (A) was 50 mV s^{-1}. EIS experiment was conducted in 0.1 M KCl solution containing 2.5 mM $Fe(CN)_6^{3-/4-}$ and the inset in (B) is the magnified EIS plots of bare GCE, p-GCE and VMSF/p-GCE.

produced on the p-GCE surface (Fig. S2†). Then, originated from the oxygen functional groups of p-GCE, VMSF can be stably prepared onto the p-GCE surface by EASA method, leading to a highly sensitive and anti-fouling electrode interface. Note that the electrochemical pretreatment and EASA processes could be performed in a very short time and the operations are simple without any tedious modification steps. Fig. 1 shows the top-view (A) and cross-section view (B) TEM images of VMSF. As revealed, VMSF possesses highly regular and uniform pores with a diameter of ~2.7 nm (Fig. 1A). No obvious defects or cracks is observed over a large domain. Cross-section view TEM image confirms that the straight nanochannels parallel to each other are oriented in one direction perpendicular to the substrate (Fig. 1B). And the homogeneous thickness of VMSF is ~88 nm. After growing VMSF onto the p-GCE surface, compact and crack-free film with several silica nanoparticle byproducts were observed (Fig. S3†), which was in agreement with those reported previously.[47]

Electrochemical characterization was employed to study the fabrication process of VMSF/p-GCE. Fig. 2A compares the cyclic voltammetry (CV) responses of $Fe(CN)_6^{3-/4-}$ at the bare GCE, p-GCE, VMSF/p-GCE and SM@VMSF/p-GCE. As seen, a pair of well-defined redox peak was displayed for $Fe(CN)_6^{3-/4-}$ at the bare GCE. After the electrochemical pretreatment of the GCE,

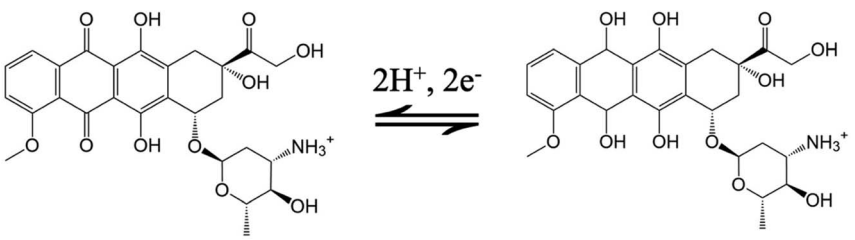

Scheme 2 Electrochemical reaction mechanism of DOX.

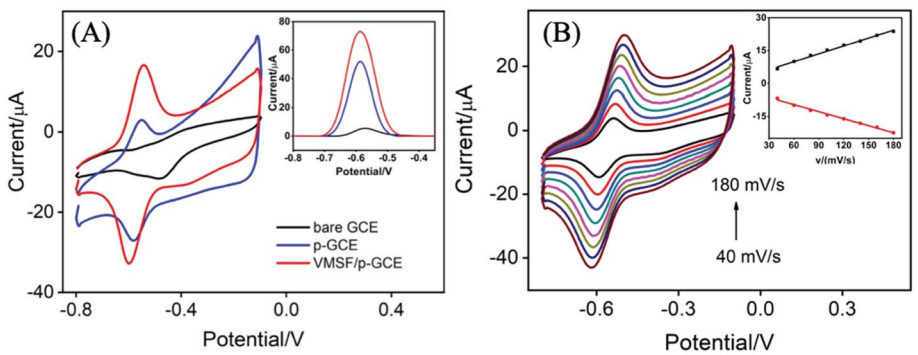

Fig. 3 (A) CV curves of bare GCE (black), p-GCE (blue) and VMSF/p-GCE (red) in 0.1 M PBS solution (pH 6.0) containing 10 μM DOX. The scan rate was 100 mV s^{-1}. Inset: corresponding DPV curves. (B) Effect of the scan rate on the CV response obtained from the VMSF/p-GCE in 0.1 M PBS (pH 6.0) containing 10 μM DOX. The inset was the dependence of anodic and cathodic peak potential on scan rate.

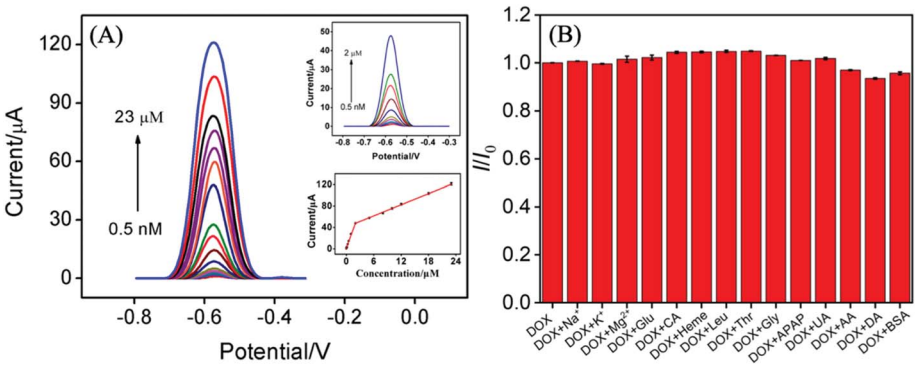

Fig. 4 (A) DPV curves of VMSF/p-GCE in 0.1 M PBS solution (pH 6.0) containing DOX ranging from 0.5 nM to 23 μM. Insets are the amplified view of the DPV curves (top) in the low-concentration region and the calibration curve (bottom). The error bars represent the standard deviation of three measurements. The concentration of DOX were 0.5 nM, 10 nM, 50 nM, 100 nM, 0.2 μM, 0.3 μM, 0.5 μM, 0.8 μM, 1 μM, 2 μM, 5 μM, 8 μM, 10 μM, 12 μM, 18 μM, 23 μM. (B) The current ratio (I/I_0) obtained from VMSF/p-GCE for detection of 10 μM DOX in the absence (I) and presence (I_0) of added interfering species. The concentration of BSA is 0.4 mg mL^{-1} and the concentration of other interfering species is 1 mM.

the current response showed slight decrease. When the p-GCE surface was coated with the SM@VMSF layer, no obvious faradaic current signals were observed, suggesting that the ingress of $Fe(CN)_6^{3-/4-}$ to the underlying p-GCE was suppressed and further proving the full coverage of VMSF on the p-GCE. By comparison, the electrochemical response of $Fe(CN)_6^{3-/4-}$ was recovered after extracting the SM from the silica nanochannels of VMSF. Arising from the negatively charged silica walls of VMSF, the transport of $Fe(CN)_6^{3-/4-}$ was electrostatically repelled, leading to the decreased signal at the VMSF/p-GCE. Moreover, the as-prepared VMSF on the p-GCE exhibits obvious charge permselectivity, suppressing negatively charge $Fe(CN)_6^{3-}$ and attracting positively charged $Ru(NH_3)_6^{3+}$ (Fig. S4†), which is due to the deprotonation of silanol groups. Fig. 2B displays the electrochemical impedance spectroscopy (EIS) plots of the bare GCE, p-GCE, VMSF/p-GCE and SM@VMSF/p-GCE in 2.5 mM $Fe(CN)_6^{3-/4-}$. The charge transfer resistance (R_{ct}) is dependent on the diameter of the semicircle in the high-frequency region. In comparison with the bare GCE, the p-GCE exhibited slightly increased semicircle diameter, confirming that the thin film containing oxygen functional groups produced on the GCE during the electrochemical pretreatment process inhibited the electron transfer. Apparently, a much larger semicircle diameter was appeared at the SM@VMSF/p-GCE, indicating the sluggish electron transfer at the interface due to the isolation of VMSF and impermeable SM. After the removal of SM, the sharply decreased semicircle diameter obtained from the VMSF/p-GCE proved that the VMSF with open channels are in favor of the electron transfer between $Fe(CN)_6^{3-/4-}$ and VMSF/p-GCE.

3.2 Electrochemical behavior of DOX at the VMSF/p-GCE

Fig. 3A records the CVs and DPVs of 10 μM DOX dissolved in 0.1 M PBS (pH 6.0) at the bare GCE, p-GCE and VMSF/p-GCE. Only weak cathodic peak current was observed at the bare GCE. The p-GCE displayed not only much more obvious redox peaks but also higher current response, which was due to the efficient electrocatalytic activity of p-GCE towards DOX. The electrochemical reaction of DOX at the electrode was shown in Scheme 2, namely the electron transfer between quinone and hydroxyquinone groups.[48] At the VMSF/p-GCE, the addition of 10 μM DOX gives rise to an apparent increase of anodic peak current by nearly 13.6-fold higher than that at the bare GCE and

Table 1 Comparison of the analytical performances of various electroanalytical methods for the determination of DOX[a]

Sensor material	Method	Range (μM)	Sensitivity (μA $μM^{-1}$)	LOD (nM)	Ref.
AgNPs-CDs-rGO/GCE	DPV	0.01–2.5	0.0829	2	51
AuNRDs/1T-MoS_2/SPE	DPV	0.01–9.5	0.8952	2.5	52
BNNS-$NiCo_2O_4$/SPE	DPV	0.01–600	0.0048	9.4	53
BPPDNi/Pt:CO-NPs/CPE	SWV	0.5–300	0.0685	100	54
OMWCNT/GCE	SWV	0.04–90	0.3919	9.4	55
HMDE	SWV	0.5–10	2.55	100	56
VMSF/ErGO/GCE	DPV	0.001–20	7.815	0.77	34
VMSF/p-GCE	DPV	0.0005–2	23.94	0.2	This work
		2–23	3.465		

[a] AuNPs, gold nanoparticles; CDs, carbon dots; rGO, reduced graphene oxide; AuNRDs, gold nanorods; 1T-MoS_2, metallic phase molybdenum disulfide; SPE, screen-printed electrode; BNNS-$NiCo_2O_4$, bird nest-like nanostructured $NiCo_2O_4$; BPPDNi, bis(1,10-phenanthroline)(1,10-phenanthroline-5,6-dione)nickel(II) hexafluorophosphate; Pt:CO-NPs, Pt:Co nanoparticle; OMWCNT, electrochemically oxidized multiwalled carbon nanotube; HMDE, hanging mercury drop electrode; ErGO, electrochemically reduced graphene oxide.

1.4-fold higher than that at the p-GCE (the inset in Fig. 3A). As reported previously,[49,50] negatively charged silica walls of VMSF resulted from the deprotonation of silanol groups (pK_a = 2–3) favor the transport of molecules with the opposite charge. And DOX in the experimental conditions carries positive charge (pK_a = 8.22).[34] By comparing the DPV responses of the used VMSF/p-GCE and p-GCE in 0.1 M PBS (pH 6.0), DOX could be electrostatically trapped into the nanochannels of VMSF, further confirming the electrostatic effect between VMSF and DOX (Fig. S5†). This memory effect could be removed by immersing the used VMSF/p-GCE electrode into 0.1 M HCl–ethanol solution under stirring for 2 min. Therefore, the advantage of VMSF/p-GCE in the analysis of DOX arises from the electrocatalytic activity of p-GCE and electrostatic preconcentration effect of VMSF. Fig. 3B shows the effect of scan rate on the redox peak currents of DOX at the VMSF/p-GCE. As can be found, both anodic and cathodic peak currents are linearly proportional to the scan rate in the range of 40 mV s^{-1} to 180 mV s^{-1}, suggesting an adsorption-controlled electrochemical process.

3.3 Electrochemical detection of DOX in buffer solution

The effects of the pH of supporting electrolyte and preconcentration time on the electrochemical performance of VMSF/p-GCE were investigated. As depicted in Fig. S6 and S7,† pH 6.0 and mechanical stirring for 50 s were adopted as the optimal experimental conditions in the following study. Moreover, the anodic and cathodic peak potentials shift linearly toward negative values with the increase of pH ranging from 4 to 8 (the inset in Fig. S6†). The slopes ($\Delta E_p/\Delta pH$) were −59.7 mV pH^{-1} and −63.6 mV pH^{-1}, demonstrating that the number of proton and electron involved in the electrochemical reaction was equal.

Fig. 4A shows the DPV responses of the VMSF/p-GCE upon successive increasing the concentrations of DOX in the range of 0.5 nM to 23 μM. The magnitude of the anodic peak current increases gradually with increasing the concentration of DOX. The corresponding calibration (the inset of Fig. 4A) displays two linear ranges, namely 0.5 nM to 2 μM and 2–23 μM. DPV curves in the low concentration range from 0–100 nM was presented in the ESI (Fig. S8†). The fitting regression equations are I (μA) = 23.94C (μM) + 1.392 (R^2 = 0.9943) and I (μA) = 3.465C (μM) + 40.78 (R^2 = 0.9988), respectively. And the limit of detection (LOD) was calculated to be 0.2 nM (S/N = 3). Moreover, Table 1 compares the analytical performances including linear range, sensitivity and LOD of the present VMSF/p-GCE with other electrochemical sensors. The VMSF/p-GCE exhibits a rather high sensitivity, a wide linear range and a low LOD.

The anti-interference ability and long-term stability of the VMSF/p-GCE was also investigated. As shown in Fig. 4B, various possible interferents including metal ions (Na^+, K^+, Mg^{2+}) and biological substances (Glu, CA, heme, Leu, Thr, Gly, APAP, UA, AA, DA and protein (BSA)) were selected and 100-fold of them (except for 0.4 mg mL^{-1} BSA) almost have no influence on the detection of 10 μM DOX. This suggests that the VMSF/p-GCE has excellent anti-interference ability. The magnitude of oxidation current value still remains 82% after eight days and the RSD of intra- and inter-day measurements were less than 5%.

3.4 Electrochemical detection of DOX in human whole blood

In order to verify the practical performance of the proposed sensor, the VMSF/p-GCE was used to detect DOX in undiluted or 50-times diluted human whole blood with 0.1 M PBS (pH 6.0). As shown in Fig. 5A, the VMSF/p-GCE exhibits sharp anodic current peak to various concentrations of DOX in 50-times diluted human whole blood sample and yields two linear ranges in the ranges of 0.5 nM to 2 μM and 2–20 μM. The sensitivities are 20.32 μA μM^{-1} and 2.696 μA μM^{-1}, respectively, which is close to that obtained in buffer solution. For comparison, the bare GCE and p-GCE were also employed to detect DOX and the results were shown in Fig. S9 and S10.† The VMSF/p-GCE presents more wider linear range, much higher sensitivity and lower LOD than that obtained at the bare GCE and p-GCE (Fig. 5B and Table S1†). It could be found that electrostatic attraction and anti-fouling ability afforded by VMSF and electrocatalytic activity of the p-GCE substrate enhance the sensitivity at the VMSF/p-GCE, displaying 19-fold higher than that at the p-GCE and 65.6-fold higher than that at the bare GCE. The

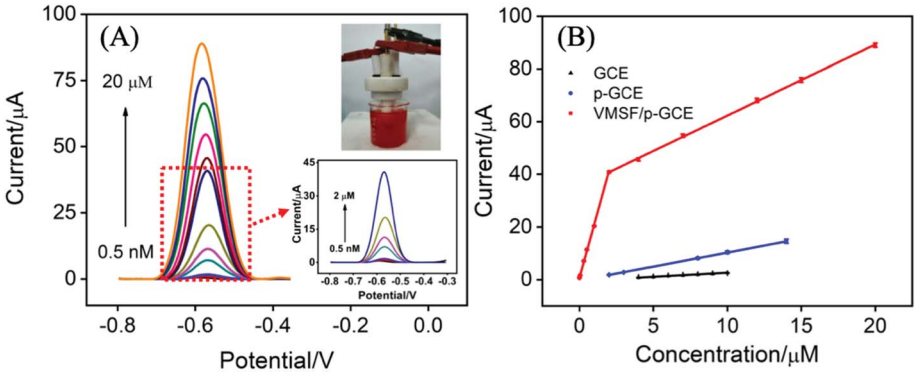

Fig. 5 (A) DPV curves of VMSF/p-GCE in 50-times diluted human whole blood sample containing various concentrations of DOX ranging from 0.5 nM to 20 μM. Insets are the real human blood sample diluted by 0.1 M PBS (pH 6.0) (top) and the amplified view of the DPV curves in the low-concentration region (bottom). (B) The linear relationship between the anodic peak currents and DOX concentration obtained at the bare GCE, p-GCE and VMSF/p-GCE. The error bars represent the standard deviation of three measurements.

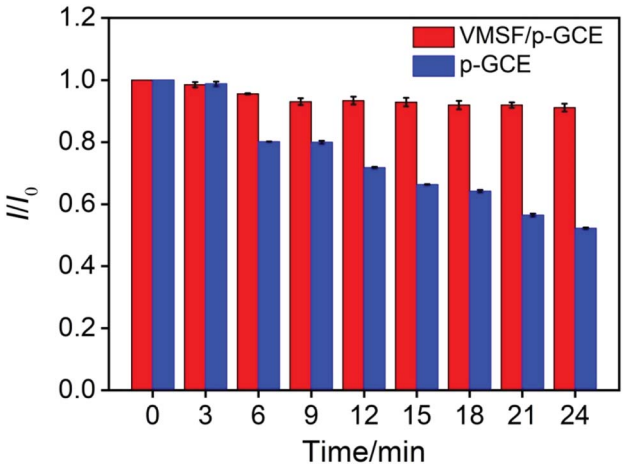

Fig. 6 Normalized oxidation peak current ratio (I/I_0) on the VMSF/p-GCE (red) and p-GCE (black) towards 5 μM DOX in 50-times diluted human whole blood sample. I and I_0 represent the anodic peak currents recorded at different time and the first detection, respectively.

anti-fouling ability of VMSF/p-GCE was further confirmed by continuously recording the current responses of the VMSF/p-GCE and p-GCE to 5 μM DOX in 50-times diluted human whole blood within 24 min. As seen in Fig. 6, the VMSF/p-GCE remains 91% of its initial signal, whereas only 52% for the p-GCE after 24 min, showing the good long-term antifouling and stability of the VMSF/p-GCE.

Fig. 7 compares the DPV curves of the bare GCE, p-GCE and VMSF/p-GCE in undiluted human whole blood sample containing 1 μM DOX. Obviously, the VMSF/p-GCE displays not only sharper anodic peak but also much higher anodic peak current than that of bare ITO and p-GCE, suggesting that the VMSF layer is able to prevent the contact of other unwanted redox interfering substances with the underlying p-GCE. Note that the complexity of undiluted human whole blood can give rise to the more serious matrix effect than diluted blood, leading to the decreased current response of DOX at the same

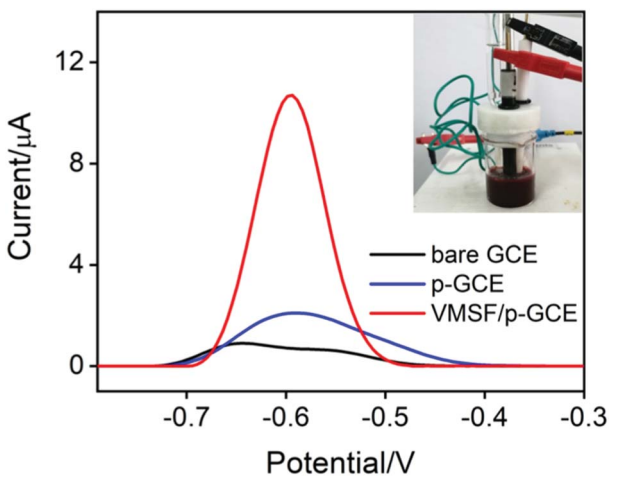

Fig. 7 DPV curves of the bare ITO, p-GCE, and VMSF/p-GCE in undiluted human whole blood sample containing 1 μM DOX. Inset is the photograph of the undiluted human blood sample.

Table 2 Recovery of DOX in undiluted human whole blood ($n = 3$)[a]

Sample	Added (μM)	Found (μM)	RSD (%)	Recovery (%)
Blood	1.00	0.963	1.7	96.3
	2.00	2.01	2.1	100.5
	10.0	9.92	1.9	99.2
	15.0	15.1	2.9	100.7

[a] Average of three detections.

concentration. In addition, satisfactory recoveries (96.3%–100.7%) and low relative standard deviations (RSD < 2.9%) were obtained at the VMSF/p-GCE for DOX detection in undiluted human whole blood sample (Table 2). All above results indicate that the VMSF/p-GCE sensor could be applied to directly and sensitively detect DOX in human whole blood, without any complex pretreatments.

4. Conclusions

In this study, a rapid and sensitive electrochemical sensor based on the p-GCE modified with VMSF has been successfully constructed for the detection of DOX in human whole blood. Electrochemical pretreatment of GCE renders the electrocatalytic activity and more oxygen-containing functional groups onto the GCE surface, allowing the stable growth of VMSF without any adhesive layer. Due to the electrocatalytic activity of p-GCE and electrostatic preconcentration effect of VMSF, the present VMSF/p-GCE sensor exhibits superior electroanalytical performance for DOX including an ultrahigh sensitivity, a wide linear range and a rather low limit of detection. The proposed method provides a simple and sensitive electrochemical method for direct analysis of human whole blood, owing to the excellent anti-fouling and anti-interference ability of VMSF. Furthermore, combination with the functionalized or nanomaterials could extend the applications of VMSF/p-GCE based sensor in the development of disposable sensors.

Conflicts of interest

There are no conflicts to declare.

Acknowledgements

This work was supported by the National Natural Science Foundation of China (21904117), the Zhejiang Provincial Natural Science Foundation of China (LY20B050007 and LY21B050003), the Science Foundation of Zhejiang Sci-Tech University (18062241-Y), and the Fundamental Research Funds of Zhejiang Sci-Tech University (2019Q060).

References

1 F. Arcamone, *Doxorubicin: anticancer antibiotics*, Elsevier, 2012.

2 W. D. Meriwether and N. R. Bachur, *Cancer Res.*, 1972, **32**, 1137–1142.
3 F. Zunino, R. Gambetta, A. Di Marco and A. Zaccara, *Biochim. Biophys. Acta*, 1972, **277**, 489–498.
4 J. Cummings, N. Willmott, B. M. Hoey, E. S. Marley and J. F. Smyth, *Biochem. Pharmacol.*, 1992, **44**, 2165–2174.
5 A. Skladanowski and J. Konopa, *Biochem. Pharmacol.*, 1994, **47**, 2279–2287.
6 C. M. Camaggi, R. Comparsi, E. Strocchi, F. Testoni and F. Pannuti, *Cancer Chemother. Pharmacol.*, 1988, **21**, 216–220.
7 K. Sakai-Kato, E. Saito, K. Ishikura and T. Kawanishi, *J. Chromatogr. B: Anal. Technol. Biomed. Life Sci.*, 2010, **878**, 1466–1470.
8 Y. Liu and B. Danielsson, *Anal. Chim. Acta*, 2007, **587**, 47–51.
9 Y. H. Liu, Y. H. Yang, X. T. Liu and T. Jiang, *Talanta*, 2008, **74**, 887–895.
10 J. S. Wang, T. Reijmers, L. J. Chen, R. Van der Heijden, M. Wang, S. Q. Peng, T. Hankemeier, G. W. Xu and J. Van der Greef, *Metabolomics*, 2009, **5**, 407–418.
11 J. Soleymani, M. Hasanzadeh, M. Eskandani, M. Khoubnasabjafari, N. Shadjou and A. Jouyban, *Mater. Sci. Eng., C*, 2017, **77**, 790–802.
12 R. Hajian, Z. Tayebi and N. Shams, *J. Pharm. Anal.*, 2017, **7**, 27–33.
13 C. Blaszykowski, S. Sheikh and M. Thompson, *Chem. Soc. Rev.*, 2012, **41**, 5599–5612.
14 A. Barfidokht and J. J. Gooding, *Electroanalysis*, 2014, **26**, 1182–1196.
15 B. L. Hanssen, S. Siraj and D. K. Y. Wong, *Rev. Anal. Chem.*, 2016, **35**, 1–28.
16 P. H. Lin and B. R. Li, *Analyst*, 2020, **145**, 1110–1120.
17 V. Urbanova and A. Walcarius, *Z. Anorg. Allg. Chem.*, 2014, **640**, 537–546.
18 F. Yan, X. Lin and B. Su, *Analyst*, 2016, **141**, 3482–3495.
19 A. Walcarius, *Curr. Opin. Electrochem.*, 2018, **10**, 88–97.
20 P. Zhou, L. Yao, K. Chen and B. Su, *Crit. Rev. Anal. Chem.*, 2020, **50**, 424–444.
21 F. Yan, W. Zheng, L. Yao and B. Su, *Chem. Commun.*, 2015, **51**, 17736–17739.
22 Q. Sun, F. Yan, L. Yao and B. Su, *Anal. Chem.*, 2016, **88**, 8364–8368.
23 F. Yan and B. Su, *Anal. Chem.*, 2016, **88**, 11001–11006.
24 B. Cheng, L. Zhou, L. Lu, J. Liu, X. Dong, F. Xi and P. Chen, *Sens. Actuators, B*, 2018, **259**, 364–371.
25 L. Lu, L. Zhou, J. Chen, F. Yan, J. Liu, X. Dong, F. Xi and P. Chen, *ACS Nano*, 2018, **12**, 12673–12681.
26 F. Yan, X. Ma, Q. Jin, Y. Tong, H. Tang, X. Lin and J. Liu, *Microchim. Acta*, 2020, **187**, 470.
27 Z. Teng, G. Zheng, Y. Dou, W. Li, C.-Y. Mou, X. Zhang, A. M. Asiri and D. Zhao, *Angew. Chem., Int. Ed.*, 2012, **51**, 2173–2177.
28 A. Walcarius, E. Sibottier, M. Etienne and J. Ghanbaja, *Nat. Mater.*, 2007, **6**, 602–608.
29 A. Goux, M. Etienne, E. Aubert, C. Lecomte, J. Ghanbaja and A. Walcarius, *Chem. Mater.*, 2009, **21**, 731–741.
30 N. A. M. Said, V. I. Ogurtsov, K. Twomey, L. C. Nagle and G. Herzog, *Procedia Chem.*, 2016, **20**, 12–24.
31 T. Nasir, L. Zhang, N. Vila, G. Herzog and A. Walcarius, *Langmuir*, 2016, **32**, 4323–4332.
32 T. Nasir, G. Herzog, M. Hebrant, C. Despas, L. Liu and A. Walcarius, *ACS Sens.*, 2018, **3**, 484–493.
33 F. Xi, L. Xuan, L. Lu, J. Huang, F. Yan, J. Liu, X. Dong and P. Chen, *Sens. Actuators, B*, 2019, **288**, 133–140.
34 F. Yan, J. Chen, Q. Jin, H. Zhou, A. Sailjoi, J. Liu and W. Tang, *J. Mater. Chem. C*, 2020, **8**, 7113–7119.
35 A. Rana, N. Baig and T. A. Saleh, *J. Electroanal. Chem.*, 2019, **833**, 313–332.
36 G. M. Swain, in *Handbook of Electrochemistry*, ed. C. G. Zoski, Elsevier, Amsterdam, 2007, pp. 111–153, DOI: 10.1016/B978-044451958-0.50006-9.
37 D. T. Fagan, I. F. Hu and T. Kuwana, *Anal. Chem.*, 1985, **57**, 2759–2763.
38 M. Poon and R. L. McCreery, *Anal. Chem.*, 1986, **58**, 2745–2750.
39 R. DeClements, G. M. Swain, T. Dallas, M. W. Holtz, R. D. Herrick and J. L. Stickney, *Langmuir*, 1996, **12**, 6578–6586.
40 J. Schreurs, J. van den Berg, A. Wonders and E. Barendrecht, *Recl. Trav. Chim. Pays-Bas*, 1984, **103**, 251–259.
41 F. Li, J. Song, D. Gao, Q. Zhang, D. Han and L. Niu, *Talanta*, 2009, **79**, 845–850.
42 S. Thiagarajan, T.-H. Tsai and S.-M. Chen, *Biosens. Bioelectron.*, 2009, **24**, 2712–2715.
43 W. Geremedhin, M. Amare and S. Admassie, *Electrochim. Acta*, 2013, **87**, 749–755.
44 J. Wang and L. D. Hutchins, *Anal. Chim. Acta*, 1985, **167**, 325–334.
45 K. Shi and K.-K. Shiu, *Anal. Chem.*, 2002, **74**, 879–885.
46 S.-J. Li, W. Guo, B.-Q. Yuan, D.-J. Zhang, Z.-Q. Feng and J.-M. Du, *Sens. Actuators, B*, 2017, **240**, 398–407.
47 L. Zhou, H. Ding, F. Yan, W. Guo and B. Su, *Analyst*, 2018, **143**, 4756–4763.
48 E. Haghshenas, T. Madrakian and A. Afkhami, *Anal. Bioanal. Chem.*, 2016, **408**, 2577–2586.
49 W. Li, L. Ding, Q. Wang and B. Su, *Analyst*, 2014, **139**, 3926–3931.
50 Q. Yang, X. Lin and B. Su, *Anal. Chem.*, 2016, **88**, 10252–10258.
51 H. J. Guo, H. Jin, R. J. Gui, Z. H. Wang, J. F. Xia and F. F. Zhang, *Sens. Actuators, B*, 2017, **253**, 50–57.
52 E. Er and N. Erk, *Microchim. Acta*, 2020, **187**, 9.
53 M. Rahimi, G. A. Bagheri and S. J. Fatemi, *J. Electroanal. Chem.*, 2019, **848**, 8.
54 S. Jahandari, M. A. Taher, H. Karimi-Maleh and G. Mansouri, *Microchim. Acta*, 2019, **186**, 7.
55 E. Haghshenas, T. Madrakian and A. Afkhami, *Anal. Bioanal. Chem.*, 2016, **408**, 2577–2586.
56 Y. Hahn and H. Y. Lee, *Arch. Pharmacal Res.*, 2004, **27**, 31–34.